Article

Developmental Cell

Znhit1 controls meiotic initiation in male germ cells by coordinating with Stra8 to activate meiotic gene expression

Graphical abstract

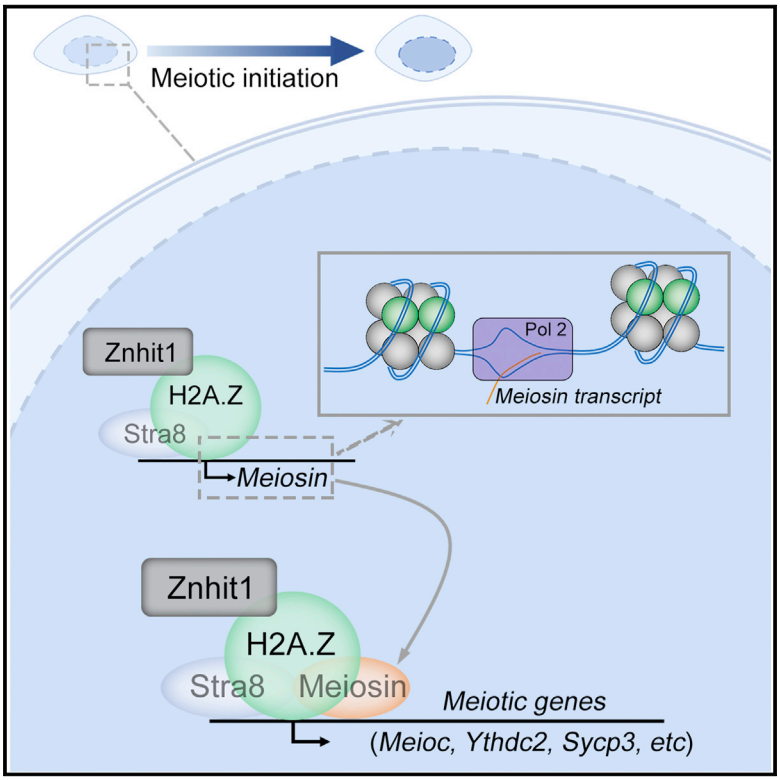

Highlights

- Inactivating *Znhit1* impairs spermatogenesis in mouse
- Znhit1 is not required for Stra8 induction but is essential for meiotic initiation
- Znhit1-dependent H2A.Z deposition is required for *Meiosin* transcription
- Znhit1/H2A.Z and Stra8 co-occupy DNA and synergistically activate meiotic gene expression

Authors

Shenfei Sun, Yamei Jiang, Qiaoli Zhang, ..., Ning Jiang, Runsheng Li, Xinhua Lin

Correspondence

bingzhao@fudan.edu.cn (B.Z.), ningjiang@fudan.edu.cn (N.J.), runshengli2007@163.com (R.L.), xlin@fudan.edu.cn (X.L.)

In brief

The mitosis-to-meiosis decision is a key step in germline development, but how chromatin regulators impact this process remains unclear. Sun et al. find that Znhit1-dependent H2A.Z deposition works together with Stra8 to regulate the entry of male germ cells into meiosis through the activation of *Meiosin* transcription.

Sun et al., 2022, Developmental Cell *57*, 901–913
April 11, 2022
https://doi.org/10.1016/j.devcel.2022.03.006

CellPress

Developmental Cell

CellPress

Article

Znhit1 controls meiotic initiation in male germ cells by coordinating with Stra8 to activate meiotic gene expression

Shenfei Sun,[1,5] Yamei Jiang,[1,5] Qiaoli Zhang,[1,4,5] Hongjie Pan,[2] Xinyang Li,[1] Li Yang,[1] Meina Huang,[2] Wei Wei,[3] Xiaoye Wang,[1] Mengdi Qiu,[1] Lihuan Cao,[1] Hua He,[3] Miao Yu,[1] Hanmin Liu,[3] Bing Zhao,[1,*] Ning Jiang,[1,*] Runsheng Li,[2,*] and Xinhua Lin[1,3,6,*]

[1]State Key Laboratory of Genetic Engineering, School of Life Sciences, Greater Bay Area Institute of Precision Medicine (Guangzhou), Zhongshan Hospital, Fudan University, Shanghai 200438, China

[2]National Health Commission (NHC) Key Laboratory of Reproduction Regulation, Shanghai Institute for Biomedical and Pharmaceutical Technologies, Shanghai 200032, China

[3]The Joint Laboratory for Lung Development and Related Diseases of West China Second University Hospital, Sichuan University and School of Life Sciences of Fudan University, Chengdu 610041, China

[4]State Key Laboratory of Reproductive Regulation and Breeding of Grassland Livestock, School of Life Sciences, Inner Mongolia University, Hohhot 010070, China

[5]These authors contributed equally

[6]Lead contact

*Correspondence: bingzhao@fudan.edu.cn (B.Z.), ningjiang@fudan.edu.cn (N.J.), runshengli2007@163.com (R.L.), xlin@fudan.edu.cn (X.L.)

https://doi.org/10.1016/j.devcel.2022.03.006

SUMMARY

The switch from mitosis to meiosis ensures the successive formation of gametes. However, it remains unclear how meiotic initiation occurs within the context of chromatin. Recent studies have shown that zinc finger HIT-type containing 1 (Znhit1), a subunit of the SRCAP chromatin remodeling complex, plays essential roles in modulating the chromatin structure. Herein, we report that the germline-conditional deletion of Znhit1 in male mice specifically blocks meiotic initiation. We show that Znhit1 is required for meiotic prophase events, including synapsis, DNA double-strand break formation, and meiotic DNA replication. Mechanistically, Znhit1 controls the histone variant H2A.Z deposition, which facilitates the expression of meiotic genes, such as *Meiosin*, but not the expression of *Stra8*. Interestingly, Znhit1 deficiency disrupts the transcription bubbles of meiotic genes. Thus, our findings identify the essential role of Znhit1-dependent H2A.Z deposition in allowing activation of meiotic gene expression, thereby controlling the initiation of meiosis.

INTRODUCTION

The dynamic interplay between transcription factors and chromatin structure is essential for cell fate determination that is regulated through the transcriptional activation or repression of tissue-specific genes (Yadav et al., 2018). In male gametogenesis, the switch from mitosis to meiosis is a specialized process for cell fate specification, which is dictated by the broad transcriptional upregulation of germline-specific genes (Handel and Schimenti, 2010; Kimble, 2011; Maezawa et al., 2020; Schultz et al., 2003; Sin et al., 2015). Male germ cells (GCs) undergo substantial chromatin reorganization upon spermatogenesis, suggesting that stage-dependent chromatin remodelers might be crucial for activating meiotic gene expression (Hammoud et al., 2014; Kimmins and Sassone-Corsi, 2005; Kota and Feil, 2010; Maezawa et al., 2018; Wang et al., 2019a). However, so far, little is known about how the chromatin remodeling processes regulate male GC development.

Meiotic entry of GCs is spatiotemporally fine-tuned by retinoic acid (RA), an active derivative of vitamin A, in both males and females (Bowles et al., 2006; Endo et al., 2019; Feng et al., 2014; Koubova et al., 2006). Genetic studies in mice have identified several key factors that control meiotic initiation, including Cyp26b1, Stra8, and Meiosin (Anderson et al., 2008; Bowles et al., 2006; Ishiguro et al., 2020). The inactivation of Cyp26b1, an RA-degrading enzyme, results in precocious GC entry into meiosis. In response to extracellular RA signaling, the GCs expressing *Dazl* initiate meiosis by inducing the expression of *Stra8*, a germline-specific transcription factor (Lin et al., 2008). Stra8 induces a transcriptional program enriched in genes involved in the regulation of the meiotic events, including G1-S phase transition, DNA replication, and meiotic prophase I (Kojima et al., 2019; Soh et al., 2015). Recent studies have reported that Meiosin (encoded by *Gm4969*), when engaged with Stra8, acts as a gatekeeper of meiotic initiation by driving the meiotic gene activation (Ishiguro et al., 2020). Moreover, negative regulators of meiotic initiation have been identified, and these include NANOS2, DMRT1, and MAX (Matson et al., 2010; Suzuki et al., 2016; Suzuki and Saga, 2008). Interestingly, a recent study reveals that nutrient restriction takes part in inducing meiotic

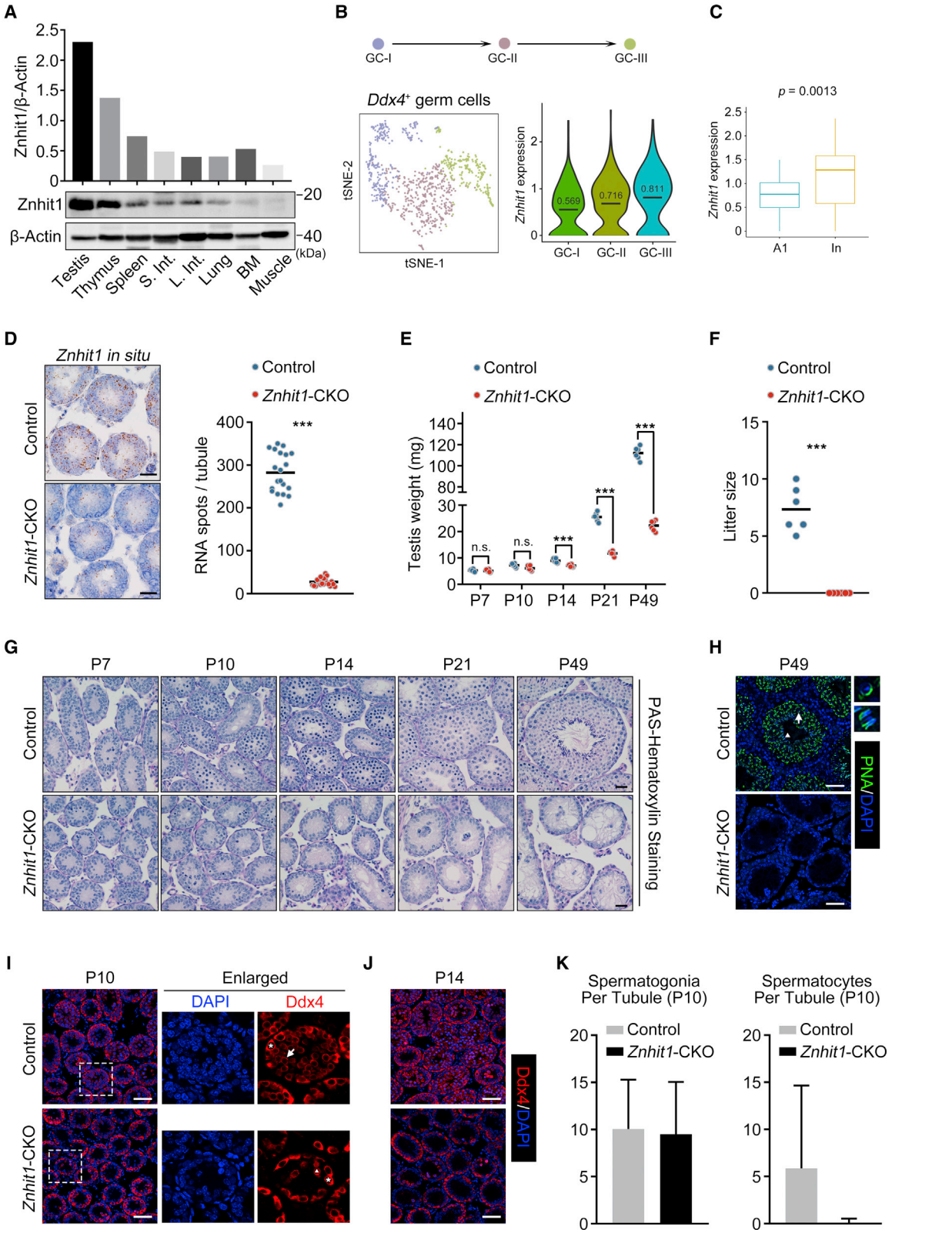

(legend on next page)

initiation *in vitro* (Zhang et al., 2021). Data from single-cell RNA sequencing (scRNA-seq) have also revealed that RA-induced *Stra8* expression marks mitosis-to-meiosis transition in the development of human germline cells (Guo et al., 2018; Hermann et al., 2018; Wang et al., 2018a; Wen and Tang, 2019), highlighting an evolutionarily conserved function that involves RA-Stra8 signaling. Although Stra8 and Meiosin are deemed essential for meiotic entry, little is known about their regulatory mechanisms.

The histone variant H2A.Z, which can replace the canonical histone H2A, has emerged as a molecular rheostat for transcriptional control and consequently cell fate specification (Murphy et al., 2018; Subramanian et al., 2015; Talbert and Henikoff, 2017). Deletion of H2A.Z in early mammalian development results in embryonic lethality, and deficient H2A.Z deposition could cause craniofacial development defects and tumorigenesis (Berta et al., 2021; Faast et al., 2001; Greenberg et al., 2019; Hood et al., 2012). H2A.Z deposition is catalyzed by the Swr1 complex in yeasts and the SRCAP complex in mammals (Clapier and Cairns, 2009; Kobor et al., 2004; Krogan et al., 2004; Mizuguchi et al., 2004; Ruhl et al., 2006; Willhoft et al., 2018; Wong et al., 2007). Zinc finger HIT-type containing 1 (Znhit1), a conserved subunit of the SNF2-related CREBBP activator protein (SRCAP) complex, plays an essential role in the incorporation of H2A.Z into genomes, thus controlling tissue development and homeostasis (Cai et al., 2005; Cuadrado et al., 2010; Feng et al., 2018; Shi et al., 2022; Sun et al., 2020; Xu et al., 2021; Ye et al., 2017; Zhao et al., 2019). Znhit1 may promote H2A.Z deposition by controlling YL1 phosphorylation (Zhao et al., 2019). During spermatogenesis, highly regulated chromatin states and nucleosome organization correlate with cell-type-specific transcriptional programs (Guo et al., 2017; Hammoud et al., 2014; Kota and Feil, 2010). Therefore, the male GC development provides an ideal model for studying the role(s) of H2A.Z deposition in gene expression and cell fate specification.

To further elucidate the mechanism(s) underlying chromatin remodeling in GC development, we generated a germline-specific Znhit1 knockout mouse strain and analyzed its role in spermatogenesis. We provide convincing evidence for an essential role of Znhit1 in meiotic initiation. Our results reveal a mechanism by which Znhit1/H2A.Z facilitates the activation of meiotic gene expression to control GC entry into meiosis. Our findings link Znhit1-dependent H2A.Z deposition and gene regulation during spermatogenesis.

RESULTS

Znhit1 is required for spermatogenesis

Analysis of transcriptome data from the mouse Encylopedia of DNA Elements (ENCODE) project (Yue et al., 2014) revealed a higher expression level of Znhit1 in the testes than other organs (Figure S1A). We first verified this by western blot (Figure 1A). Then, we queried published scRNA-seq data of post-natal day 7 (P7) male GCs for *Znhit1* expression (Wang et al., 2019b). *Ddx4*$^{+}$ GCs could be partitioned into three subsets, based on key gene expression signatures (*Gfra1*, *Plzf*, *Kit*, *Stra8*, and *Meioc*): GC-I, -II, and -III (Figures 1B and S1B). GC-I is undifferentiated spermatogonial stem cells (SSCs), whereas GC-II and -III are two differentiating spermatogonia subsets. This signified a meiotic commitment order of early spermatogenesis (Figure S1B). Interestingly, the expression of *Znhit1* increased from GC-I to GC-III (Figure 1B). Consistent with this observation, examination of scRNA-seq data from synchronous spermatogenic cells (Chen et al., 2018) demonstrated that *Znhit1* was upregulated during the type A1 to intermediate (In) spermatogonia transition (Figure 1C). These data suggest possible functions of Znhit1 in the early cell fate specification during spermatogenesis.

To examine the functions of Znhit1 in spermatogenesis, we generated *Znhit1*$^{fl/fl}$; *Ddx4-cre* mice in the C57BL/6J background to achieve a conditional GC knockout of Znhit1 ("*Znhit1*-conditional knockout (CKO) mice" hereinafter). RNA *in situ* hybridization and western blot confirmed that Znhit1 was depleted in the GCs of *Znhit1*-CKO mice but not in somatic cells, e.g., Sertoli cells (Figures 1D and S1C). Although *Znhit1*-CKO males maintained normal body weight, their testes were smaller than those of their littermate controls (Figures 1E and S1D). In addition, *Znhit1*-CKO males were infertile (Figure 1F).

Next, we performed periodic acid-Schiff (PAS)-hematoxylin staining on the testis sections at P7, P10, P14, P21, and P49. As shown in Figure 1G, there was no difference between the testicular tubules of the control and *Znhit1*-CKO mice at P7. For control mice, preleptotene spermatocytes started to appear in the cavity of seminiferous tubules after P10. In contrast, *Znhit1*-CKO males had almost no spermatocytes from P10 to P49. Ddx4 (also known as Vasa) is a putative marker of both male and female GCs (Raz, 2000), and anti-Ddx4 immunostaining showed that the number of Ddx4-positive spermatocytes was markedly reduced, as opposed to the number of spermatogonia in *Znhit1*-CKO males (Figures 1I–1K). Peanut agglutinin (PNA)

Figure 1. Znhit1 deletion impairs spermatogenesis

(A) Western blotting of Znhit1 in wild-type mouse tissues. β-Actin served as a loading control. Quantitative data are shown in the upper panel. S. Int., small intestine; L. Int., large intestine; BM, bone marrow.

(B) Three subsets of *Ddx4*$^{+}$ germ cells from scRNA-seq data. Relative *Znhit1* expression levels in three subsets are shown in the right panel.

(C) Relative *Znhit1* expression in type A1 spermatogonia (A1) and type intermediate spermatogonia (In).

(D) *Znhit1 in situ* hybridization in P10 testis sections. Scale bars, 20 μm. Quantitative data are shown in the right panel.

(E) Weights of testes obtained from control or *Znhit1*-CKO mice at indicated times (n = 6).

(F) Litter sizes when control or *Znhit1*-CKO males were mated with wild-type females (n = 6).

(G) Histological testicular sections in control or *Znhit1*-CKO mice at indicated times. Scale bars, 20 μm.

(H) Immunostaining of PNA in testis sections from control or *Znhit1*-CKO mice at indicated times. Arrows indicate rounding spermatids, and triangles indicate elongating spermatids. Scale bars, 50 μm.

(I and J) Immunostaining of Ddx4 in testis sections from control or *Znhit1*-CKO mice at indicated times. Asterisks indicate spermatogonia, arrows indicate spermatocytes, and triangles indicate apoptotic cells. Scale bars, 50 μm.

(K) Quantitative data of Ddx4 immunostaining results. All images are representative of n = 3 mice per genotype. Data are presented as the mean ± SD. ***p < 0.001. See also Figure S1.

immunostaining further confirmed the absence of round spermatids and elongating spermatids in the *Znhit1*-CKO testes (Figure 1H). Collectively, our data demonstrate that Znhit1 is required for spermatogenesis.

Znhit1 is not required for spermatogonial maintenance and differentiation

To define the role(s) of Znhit1 in spermatogenesis, we used the immunostaining assay of molecular markers to dissect GC fates in Znhit1 mutants. Plzf acts as a spermatogonia-specific transcription factor and is required for SSC self-renewal (Buaas et al., 2004; Costoya et al., 2004). As shown in Figure 2A, $Plzf^+$ spermatogonia were unaffected following Znhit1 deletion. In addition, the inactivation of Znhit1 in GCs did not affect the identity of $Sox9^+$ Sertoli cells (Figure S2A). $GFR\alpha1^+$ spermatogonia have been identified to comprise the stem cell pool in testes (Nakagawa et al., 2010). Interestingly, $GFR\alpha1^+$ SSCs were unaffected by the *Znhit1* knockout (Figure 2B). *Znhit1*-CKO males also displayed a normal appearance in terms of Kit^+ differentiating spermatogonia (Figure 2C). Consistently, no difference was observed in the expression of SSC self-renewal genes (i.e., *Oct4*, *Gfra1*, *Etv5*, and *Bcl6b*) and differentiating genes (i.e., *Dmrt1*, *Ngn3*, *Kit*, and *Sohlh2*) between control and Znhit1 mutants, as measured by RT-qPCR (Figure 2D). These results suggest that Znhit1 is not essential for spermatogonial maintenance and differentiation.

Znhit1 is not required for Stra8 induction but is essential for meiotic initiation

Following spermatogonial differentiation, male GCs initiate their entry into meiosis. Next, we examined whether Znhit1 is required for meiotic initiation. Immunostaining of Stra8, a marker for differentiating spermatogonia and preleptotene spermatocytes, showed that $Plzf^+Stra8^+$ spermatogonia were present in both control and Znhit1 mutant testes. However, $Plzf^-Stra8^+$ preleptotene spermatocytes, localized in the cavity of seminiferous tubules of the control testes, were rarely observed in P10 and P14 *Znhit1*-CKO testes (Figure 2E), which indicates that Znhit1 deletion blocked meiotic initiation. We also examined the expression of Dazl, which is required for *Stra8* transcription (Lin et al., 2008). As shown in Figure 2F, no difference in Dazl expression was observed in *Znhit1*-deficient GCs. These results present an intriguing phenotype: although Dazl and Stra8 were normally expressed, Znhit1 knockout led to meiotic initiation defects. To further characterize the fate of the $Znhit1^{-/-}$ GCs, we performed the terminal dUTP nick-end labeling (TUNEL) staining and found that more GCs in Znhit1 mutant testes were TUNEL-positive, indicating that these aberrant cells were removed by the apoptotic pathway (Figure 2G). These results suggest that the loss of Znhit1 impairs GC entry into meiosis.

The hallmark of meiotic initiation is defined by DNA double-strand break (DSB) formation and homologous synapsis (Zhang et al., 2021). Immunostaining for γH2AX, a marker of DSB loci, revealed that the formation of DSB was impaired in *Znhit1*-deficient GCs, as compared with controls (Figures 3A and 3A′). Furthermore, we performed immunostaining for Sycp3, a synaptonemal complex protein. Compared with controls, the Sycp3 signal was almost absent in *Znhit1*-CKO testes (Figures 3B, 3B′, and S2B), demonstrating that Znhit1 was required for the formation of the synaptonemal complex.

DNA is replicated immediately before GCs process into meiotic prophase I (Baltus et al., 2006). Therefore, we injected bromodeoxyuridine (BrdU) into P10 control and *Znhit1*-CKO males and then determined the rate of BrdU incorporation into newly replicated DNA. As shown in Figures 3C and 3C′, $BrdU^+Stra8^+$ preleptotene spermatocytes were absent in the *Znhit1*-CKO testes, in comparison with the controls, indicating that premeiotic DNA replication was disrupted in the absence of Znhit1 activity.

Taken together, these results provide strong evidence that Znhit1 is essential for meiotic initiation.

Znhit1 controls the transcription of meiotic genes

To identify the regulatory mechanisms of Znhit1 in meiotic initiation, we performed RNA-seq analysis using P10 control and *Znhit1*-CKO testes. The RNA-seq data from three biological replicates yielded 1,719 differentially expressed genes (DEGs) (Figure 4A; Table S1). Gene ontology (GO) analysis highlighted an alteration of the expression of genes involved in regulating the meiotic cell cycle, synapsis, and male meiosis (Figure 4B; Table S2). Consistent with the defects in meiotic initiation, gene set enrichment analysis (GSEA) indicated that Znhit1 deletion resulted in a dramatically decreased enrichment of upregulated genes during meiosis (Figure 4C; Table S3). Specifically, a large number of meiotic genes were downregulated in Znhit1 mutants, and these genes were involved in the G1-S phase transition, DNA replication, and many aspects of meiotic prophase I, including DSB and repair, chromosome condensation and movement, and homologous pairing and recombination (Figures 4F and S3A). These results suggest that Znhit1 is involved in meiotic gene expression.

The activation of the meiotic transcriptional program is dependent on the expression and function of transcriptional activator Stra8 (Kojima et al., 2019). Importantly, although Stra8 expression was not affected, Stra8 target genes were markedly repressed in *Znhit1*-deficient GCs (Figure 4D; Table S3), suggesting a possible function of Znhit1 in regulating Stra8 activities during meiotic initiation. Moreover, RNA-seq data revealed that a Stra8 cofactor, *Meiosin*, was dramatically downregulated in Znhit1 mutant cells. Consistently, we also observed that Meiosin target genes were downregulated in the *Znhit1*-CKO testes (Figure 4E; Table S3). These data suggest that Znhit1 may regulate Stra8 activities by controlling the expression of *Meiosin*.

To further examine the involvement of Znhit1 in *Meiosin* transcription, we performed RT-qPCR assay and found that the number of transcripts of *Meiosin*, and its downstream targets (i.e., *Meioc*, *Ythdc2*, and *Sycp3*), was also reduced in *Znhit1*-deficient differentiating spermatogonia compared with controls (Figures 4G, S3B, and S3C), further suggesting that Znhit1 regulates *Meiosin* transcription during the onset of meiosis.

Taken together, our results argue that Znhit1 controls meiotic gene expression via upregulating *Meiosin*, but not *Stra8*.

Znhit1 deletion causes blockage of transition of differentiating spermatogonia into spermatocytes

Next, we sought to define the gene expression profile of male GCs following Znhit1 deletion using scRNA-seq. A total of

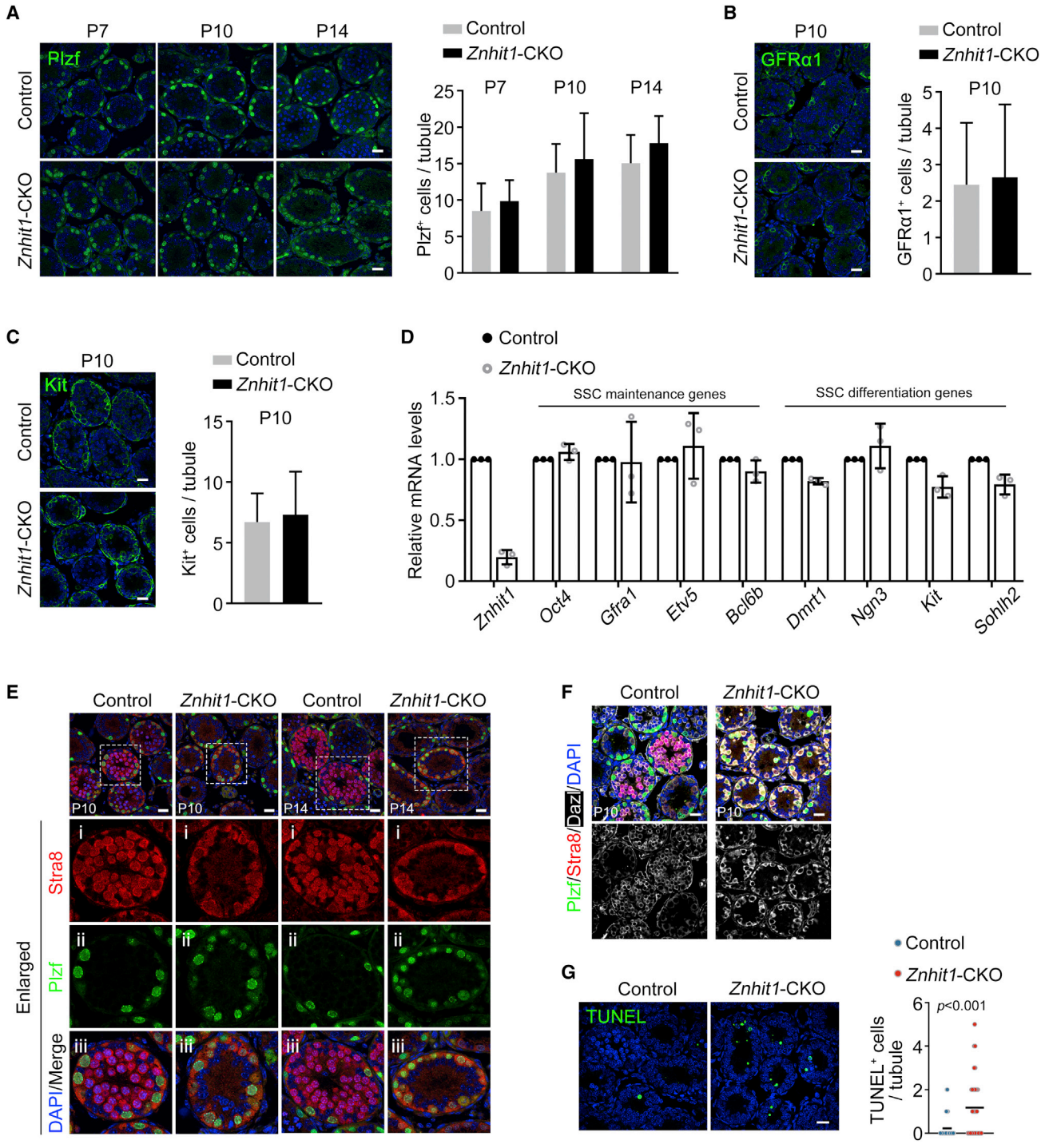

Figure 2. Znhit1 controls meiotic initiation

(A) Immunostaining for Plzf in testis sections in control or *Znhit1*-CKO mice at indicated times. Quantitative data are shown in the right panel.

(B) Immunostaining for GFRα1 in testis sections from control or *Znhit1*-CKO mice at indicated times. Quantitative data are shown in the right panel.

(C) Immunostaining of Kit in testis sections from control or *Znhit1*-CKO mice at indicated times. Quantitative data are shown in the right panel.

(D) RT-qPCR analysis of indicated genes in testes from P10 control or *Znhit1*-CKO mice (n = 3).

(E) Immunostaining of Stra8 and Plzf in testis sections from control or *Znhit1*-CKO mice at indicated times.

(F) Immunostaining of Stra8, Plzf, and Dazl in testis sections from control or *Znhit1*-CKO mice at indicated times.

(G) TUNEL staining in testis sections from P10 control or *Znhit1*-CKO mice. All images are representative of n = 3 mice per genotype. Data are presented as the mean ± SD. Scale bars, 20 μm. See also Figure S2 and Table S4.

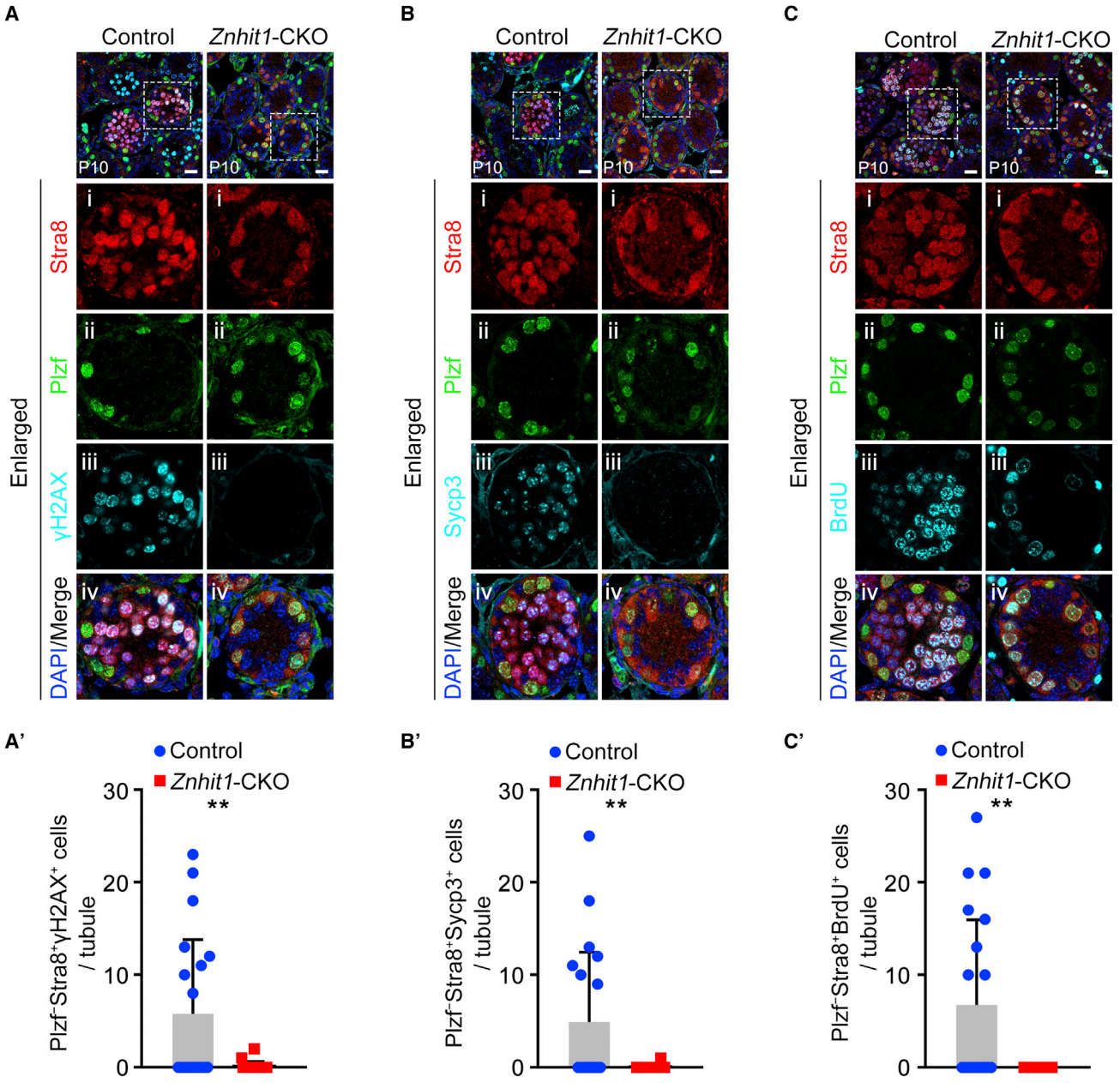

Figure 3. Znhit1 is essential for meiotic prophase events

(A and A′) Immunostaining of Stra8, Plzf, and γH2AX in testis sections of control or *Znhit1*-CKO mice at indicated times.

(B and B′) Immunostaining of Stra8, Plzf, and Sycp3 in testis sections of control or *Znhit1*-CKO mice at indicated times.

(C and C′) Immunostaining of Stra8, Plzf, and BrdU in testis sections from control or *Znhit1*-CKO mice at indicated times. All images are representative of n = 3 mice per genotype. Scale bars, 20 μm. Data are presented as the mean ± SD. **p < 0.01. See also Figure S2.

3,005 control and 4,500 Znhit1$^{-/-}$ testicular cells were analyzed, and cell populations were visualized by uniform manifold approximation and projection (UMAP) for dimension reduction (Figure S4A). Upon clustering the control testicular cells with the cells obtained from *Znhit1*-CKO mice, we found that the *Ddx4*$^{+}$ GCs in Znhit1$^{-/-}$ testicular cells developed to *Plzf*^{low} *Kit*^{high} differentiating spermatogonia, but not *Piwil1*$^{+}$ spermatocytes and *Sun5*$^{+}$ spermatids (Figures S4B and S4C). Consistently, scRNA-seq data revealed that meiotic genes, including *Meiosin*, were repressed in *Znhit1*-deficient spermatogonia (Figure S4D). These results indicate that Znhit1 deletion blocks meiotic initiation by arresting male germline cells at the differentiating spermatogonia state.

Znhit1/H2A.Z and Stra8 co-occupy the TSS region and drive the meiotic transcriptional program

To determine the mechanism by which Znhit1 drives the expression of meiosis-related genes, we performed chromatin

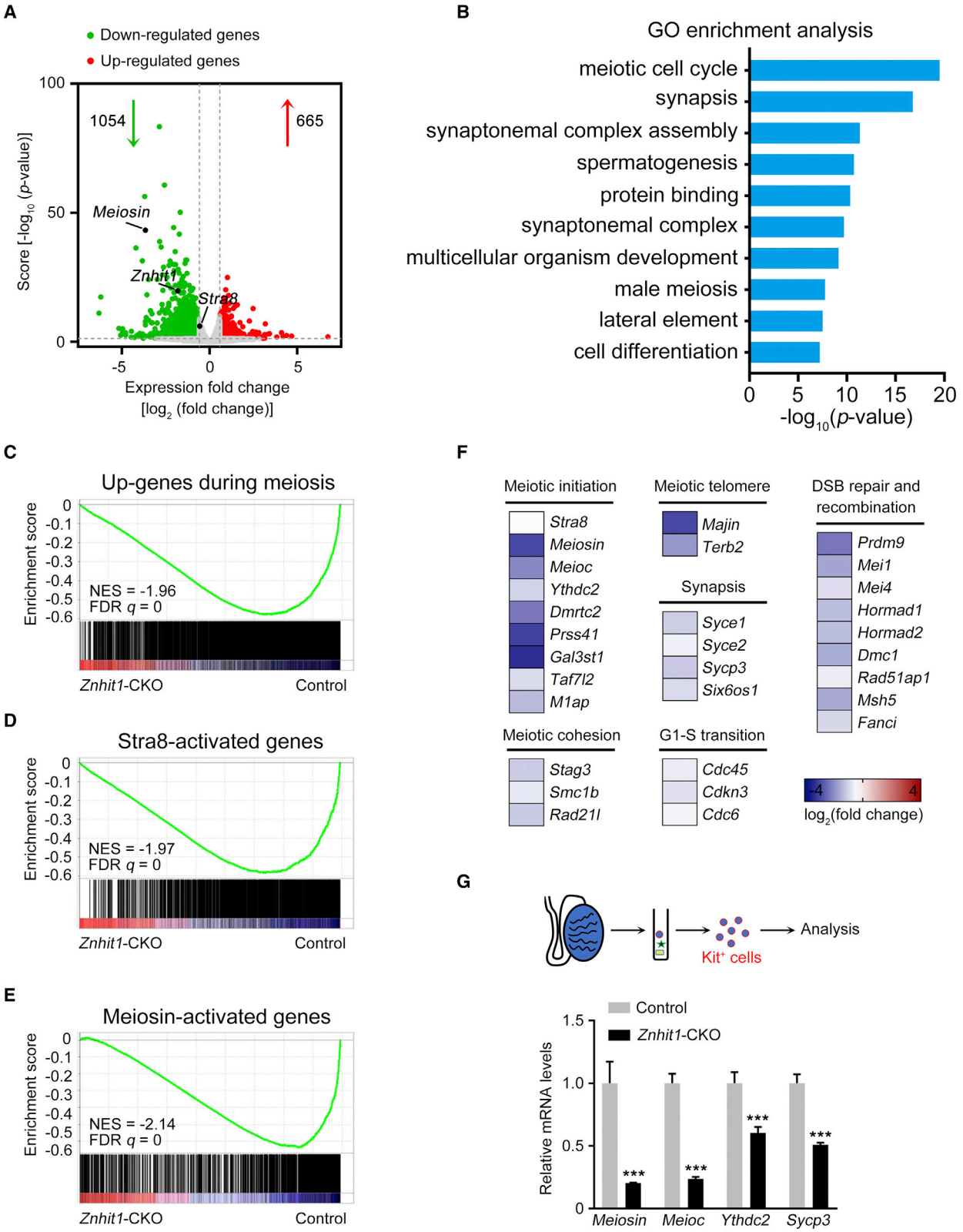

Figure 4. Znhit1 is required for meiotic gene expression

(A) Volcano plot of differentially expressed genes (DEGs) after Znhit1 deletion (n = 3).

(B) Gene ontology (GO) analysis of DEGs highlighting changed biological processes after *Znhit1* deletion.

(legend continued on next page)

immunoprecipitation followed by sequencing (ChIP-seq) in P10 testes for the histone variant H2A.Z. The ChIP-seq data from wild-type testes revealed 14,992 H2A.Z-binding sites that correspond to 12,269 genes, most (72.5%) of which were within the transcription start site (TSS) regions and distributed in a bimodal pattern (Figures 5A and 5B). Although the total H2A.Z protein level was unchanged, Znhit1 deletion led to a genome-wide loss of H2A.Z binding, confirming the dominant role of Znhit1 in global H2A.Z deposition (Figures 5B and S5A). Correlation analysis with RNA-seq data from WT and *Znhit1*-CKO testes demonstrated that 1,102/1,719 (64.1%) of Znhit1-regulated DEGs were bound by H2A.Z, suggesting that more than half of these dysregulated genes were the direct targets of Znhit1/H2A.Z (Figure 5C).

To further verify the loss of H2A.Z on meiotic gene promoters, we sorted Kit$^+$ spermatogonia and performed the cleavage under targets and tagmentation (CUT&Tag) assay against H2A.Z (Kaya-Okur et al., 2019). As shown in Figure 5D, Znhit1 deletion led to the removal of H2A.Z incorporation into the TSS regions of *Meiosin* and its targets, including *Meioc* and *Sycp3*. These findings suggest that Znhit1 might directly control *Meiosin* transcription by regulating H2A.Z TSS incorporation.

Meiotic initiation is strictly dependent on the transcriptional activator Stra8, so we further compared the genome-wide distribution of H2A.Z and Stra8. Analysis of published Stra8 ChIP-seq data (Kojima et al., 2019) revealed 8,467 significant peaks, among which 4,059 (47.9%) of these binding sites were co-occupied with H2A.Z and 3,233/4,059 (79.7%) cobinding sites were within the TSS regions (Figures 5E and S5B). At the genome-wide level, Stra8 enrichment was also significantly correlated with H2A.Z (r = 0.57, Figure S5C). The TSS regions occupied by Stra8 or H2A.Z showed enrichment for consensus binding motifs for many transcriptional regulators, including YY1, SP5, and SP1 (Figure S5D). Notably, the H2A.Z/Stra8 co-occupied genes included a subset of essential meiotic genes, such as *Meiosin*, *Meioc*, *Mei1*, *Majin*, and *Smc1b* (Figures 5F and S5E). Furthermore, Znhit1-regulated genes with H2A.Z/Stra8 co-occupancy in the TSS regions were significantly downregulated, compared with other DEGs (Figure 5G), suggesting that their cobinding may synergistically activate meiotic gene expression. These data suggest that H2A.Z and Stra8 co-occupy the TSS regions and synergistically activate the transcription of meiotic genes.

Znhit1/H2A.Z modulates transcription bubbles of meiotic genes

We next asked how Znhit1/H2A.Z regulates gene expression at the molecular level. One possibility is that H2A.Z TSS enrichment may take part in regulating transcription initiation. Previous studies in *Drosophila* have shown that Dmp18, a homolog of Znhit1, physically interacts with the TFIIH complex through Dmp52 (Herrera-Cruz et al., 2012). It has been known that TFIIH plays an essential role in the initiation of transcription by opening promoter DNA (He et al., 2013). Kethoxal-assisted single-stranded DNA sequencing (KAS-seq) allows the measurement of transcription bubbles at the genome-wide scale (Wu et al., 2020), and we investigated whether Znhit1/H2A.Z loss affected the formation of transcription bubbles by performing KAS-seq (Figures 6A and 6B). We observed that the TSS regions of Znhit1-regulated meiotic genes, including *Meiosin*, *Meioc*, and *Sycp3*, showed a substantial decrease in transcription bubbles following Znhit1 deletion (Figures 6C–6E). In contrast, somatic genes, including *Gapdh* and *Tuba1a*, showed no difference (Figures S6A and S6B). These results demonstrate that Znhit1/H2A.Z is required for the transcription initiation of meiotic genes, possibly by regulating the opening of TSS DNA.

DISCUSSION

Meiotic entry in GCs is a highly regulated process of cell fate specification; however, how chromatin dynamics contribute to this process is poorly understood. In this study, using a conditional knockout mouse model combined with molecular and genomic approaches, we have provided functional and molecular evidence that Znhit1 acts as a critical regulator of meiotic initiation. Our results provide insights into how specific chromatin structures determine cell fate.

Znhit1 selectively controls meiotic initiation

One important issue in cell biology is how epigenetic regulators modulate GC specification during the mitosis-to-meiosis transition that is accompanied by massive chromatin remodeling (Kimmins and Sassone-Corsi, 2005; Kota and Feil, 2010). Previous studies have shown that histone modifications, mediated by polycomb repressive complex 1 (PRC1), play a role in the regulation of meiotic initiation and the deficiency of Rnf2, a PRC1 component, causes female primordial GCs to enter into meiosis precociously (Yokobayashi et al., 2013). Unlike what has been observed for oogenesis, the loss of Rnf2 in the male germline disrupts the differentiation of spermatogenic cells that occurs before meiotic initiation (Maezawa et al., 2017). Therefore, it remains largely unclear how epigenetic regulators control the entry of male GCs into meiosis. In our study, we conditionally knocked out Znhit1 in early germline development and found that Znhit1 is dispensable for spermatogonial maintenance or differentiation. Interestingly, Znhit1 is upregulated before the onset of meiosis, suggesting its primary role in meiotic initiation. Consistent with this observation, our results show that meiotic initiation is severely blocked following the loss of Znhit1. Thus, our study identifies Znhit1 as a critical epigenetic regulator of meiotic initiation in male GC development.

Znhit1 regulates the expression of Meiosin but not Stra8

How does Znhit1 regulate meiotic initiation? One possibility is that Znhit1 may control the expression or activities of Stra8.

(C–E) GSEA of RNA-seq data for the control and *Znhit1*-CKO testicular cells. Selected gene sets encoded products related to upregulated genes during meiosis, Stra8-activated genes, or Meiosin-activated genes (n = 3 biologically independent samples for each group; FDR q < 25%). NES, normalized enriched score.
(F) Heatmap depicting downregulated genes identified by GO analysis. Stra8 served as a control.
(G) RT-qPCR analysis of indicated genes in Kit$^+$ differentiating spermatogonia from P10 control or *Znhit1*-CKO mice. Data are presented as the mean ± SD. ***p < 0.001. See also Figures S3 and S4 and Tables S1–S4.

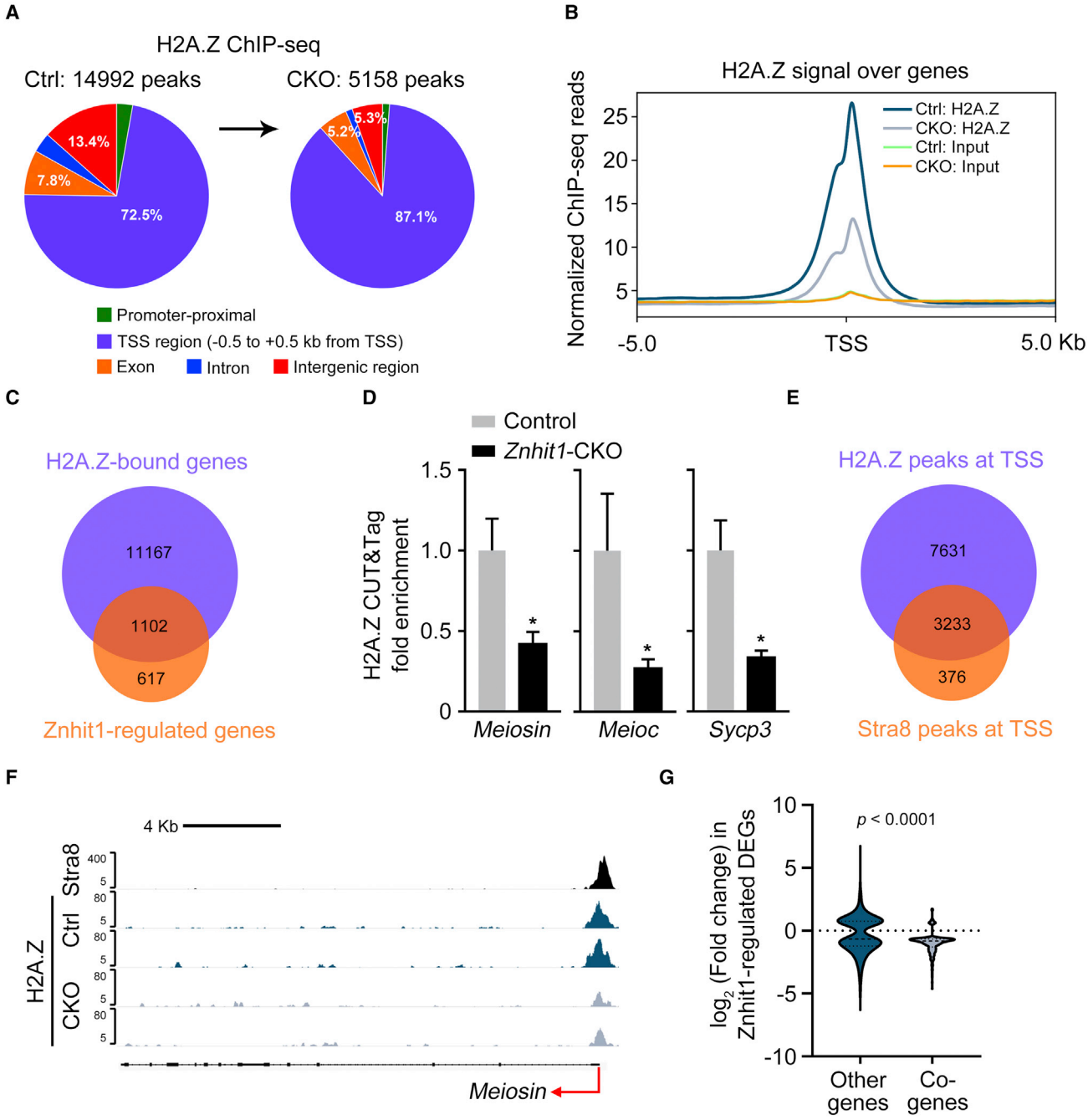

Figure 5. Znhit1-dependent H2A.Z incorporation colocalizes with the transcriptional activator Stra8

(A) Distribution of H2A.Z binding sites in the genome in control (Ctrl) or *Znhit1*-CKO (CKO) testicular cells (n = 2).

(B) Normalized signal density of H2A.Z relative to input in control (Ctrl) or *Znhit1*-CKO (CKO) testes.

(C) Venn diagram showing the overlap between H2A.Z-bound genes and DEGs in control and *Znhit1*-CKO testicular cells.

(D) H2A.Z CUT&Tag assay showing the fold enrichment of H2A.Z in the TSS region of indicated genes in Kit$^+$ spermatogonia.

(E) Venn diagram showing the overlap between H2A.Z-bound TSS and Stra8-bound TSS.

(F) Representative H2A.Z ChIP-seq tracks at the *Meiosin* locus in control (Ctrl) or *Znhit1*-CKO (CKO) testicular cells, compared with Stra8.

(G) Znhit1-regulated DEGs were classified into two groups based on whether their TSS regions were co-occupied with H2A.Z and Stra8 (co-genes) or not (other genes). Overall expression levels were compared. Data are presented as the mean ± SD. *p < 0.05. See also Figure S5 and Table S5.

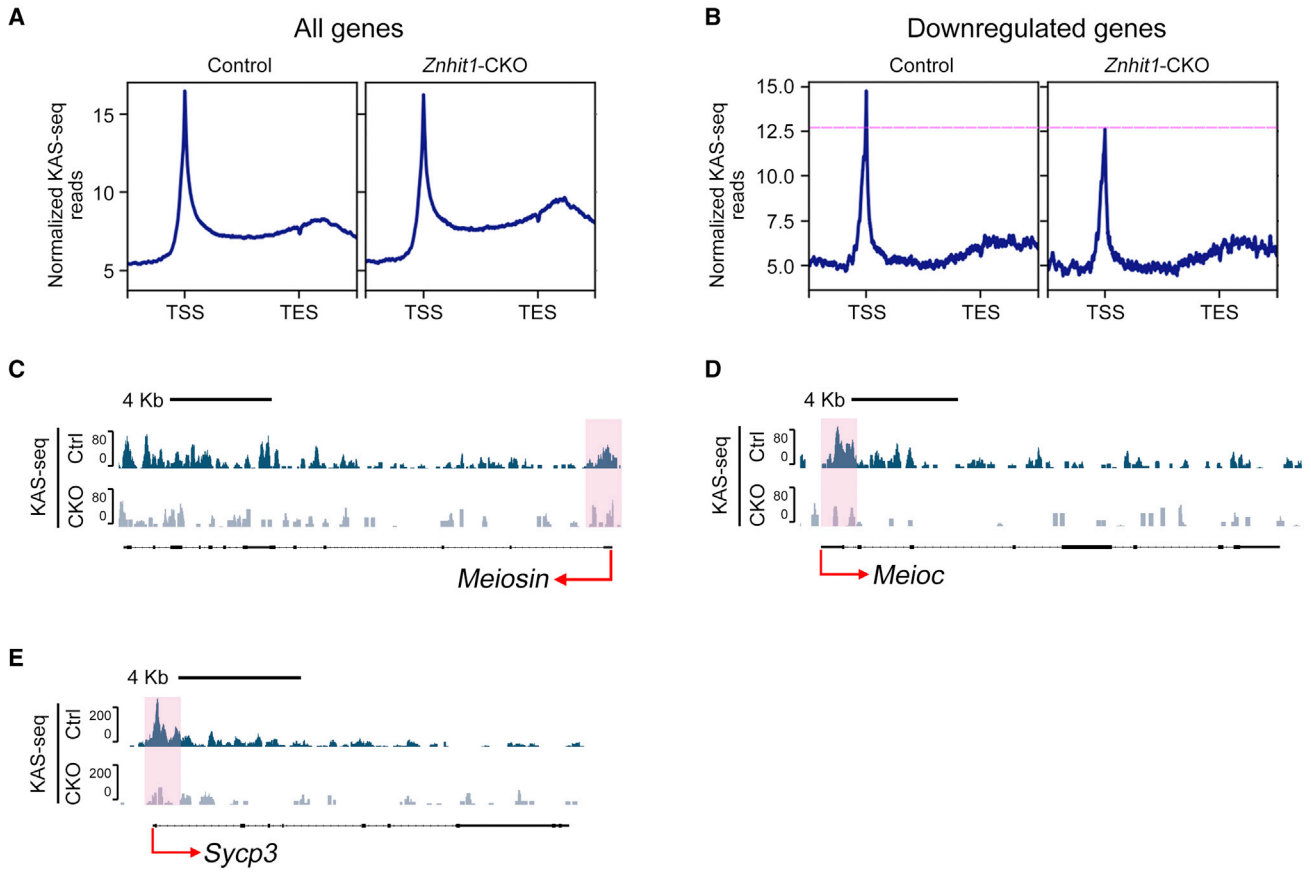

Figure 6. Znhit1 modulates transcription bubble formation

(A and B) Normalized signal density via KAS-seq in all genes (A) or downregulated genes (B).

(C–E) Representative KAS-seq tracks at the *Meiosin*, *Meioc*, and *Sycp3* loci in control (Ctrl) or *Znhit1*-CKO (CKO) testicular cells. See also Figure S6.

Interestingly, we found that Znhit1-mediated H2A.Z deposition is required for Stra8 activities but not its expression. Our results reveal that Znhit1 deletion impairs the expression of Stra8-target genes in male GCs (Figure 4D). Importantly, we show that the loss of Znhit1 reduces the expression of Meiosin, a cofactor of Stra8. Recent studies have demonstrated that Meiosin physically interacts with Stra8 and that Meiosin is indispensable for the transcription regulatory activities of Stra8 (Ishiguro et al., 2020). Thus, our results argue that Znhit1 controls the activities of Stra8 by regulating Meiosin expression.

Znhit1/H2A.Z regulates the formation of transcription bubbles

The functions of the histone variant H2A.Z in gene regulation have gained much attention, but its exact roles remain largely unclear (Giaimo et al., 2019; Talbert and Henikoff, 2017). Utilizing Znhit1 conditional knockout mice and genomic technologies (i.e., ChIP-seq and KAS-seq), we demonstrated that the transcription bubbles of meiotic genes would decrease significantly in the absence of H2A.Z binding. This finding indicates that Znhit1-mediated H2A.Z deposition plays an important role in transcription initiation by opening promoter DNA. Thus, our data shed light on how H2A.Z promoter enrichment contributes to gene regulation.

In the light of current data, we propose a model by which Znhit1-dependent H2A.Z deposition, engaged with Stra8, activates the transcription of *Meiosin* to promote a burst of meiotic gene expression. These findings may be conducive to the generation of *in vitro*-derived GCs.

Limitations of the study

RA signaling acts as one of the prominent driving forces in meiotic initiation during spermatogenesis (Bowles et al., 2006; Tong et al., 2013). In this study, we have shown that Znhit1 plays a pivotal role in controlling the entry of male GCs into meiosis. On one hand, we observed that the expression of Znhit1 is upregulated before meiotic initiation. On the other hand, previous studies have shown that the histone variant H2A.Z could be redeposited upon treatment of RA in embryonic stem cells (Chen et al., 2013; Wang et al., 2018b). These suggest that there may be a functional connection between RA-gradient and Znhit1/H2A.Z in male germline development. Further experiments utilizing the RA synthesis inhibitor WIN 18,446 (Romer et al., 2018) would help address this question. Given that Znhit1 is an evolutionarily conserved protein, further investigations would be necessary to address whether Znhit1 controls meiotic initiation in other vertebrates including humans. In addition, the function(s) of Znhit1 in oogenesis remains an open question.

STAR★METHODS

Detailed methods are provided in the online version of this paper and include the following:

- KEY RESOURCES TABLE
- RESOURCE AVAILABILITY
  - Lead contact
  - Materials availability
  - Data and code availability
- EXPERIMENTAL MODEL AND SUBJECT DETAILS
- METHOD DETAILS
  - Histology
  - TUNEL assay
  - RNAscope in situ hybridization
  - Isolation of Kit$^+$ spermatogonia
  - Quantitative RT-PCR (RT-qPCR)
  - Western blot
  - RNA-seq
  - ChIP-seq and KAS-seq
  - CUT&Tag
  - Single-cell RNA sequencing (scRNA-seq)
- QUANTIFICATION AND STATISTICAL ANALYSIS

SUPPLEMENTAL INFORMATION

Supplemental information can be found online at https://doi.org/10.1016/j.devcel.2022.03.006.

ACKNOWLEDGMENTS

We thank Ming-Han Tong for critical discussions, Chuan He for N_3-kethoxal, and Weixu Wang for help in bioinformatic analysis. This work was supported by grants from the National Key Research and Development Program of China (2018YFC1003500, 2018YFA0800100, and 2021YFC2501800), the National Natural Science Foundation of China (31730044, 32192403, 81971443, and 31900591), the Science and Technology Major Project of Inner Mongolia Autonomous Region of China to the State Key Laboratory of Reproductive Regulation and Breeding of Grassland Livestock (2020ZD0008), and the Shanghai Municipal Health Commission (20194Y0343).

AUTHOR CONTRIBUTIONS

S.S. and X.L. conceived and designed the study; S.S. performed most of the experiments with the help from Y.J., Q.Z., H.P., X.L., L.Y., M.H., W.W., X.W., M.Q., L.C., H.H., H.L., and B.Z.; Y.J. performed scRNA-seq under the guidance of M.Y.; N.J. performed the bioinformatics analysis; X.L. and R.L. supervised the work; and S.S. and X.L. wrote the manuscript, with contributions from all authors.

DECLARATION OF INTERESTS

The authors declare no competing interests.

Received: April 27, 2021
Revised: January 25, 2022
Accepted: March 10, 2022
Published: April 11, 2022

REFERENCES

Anderson, E.L., Baltus, A.E., Roepers-Gajadien, H.L., Hassold, T.J., de Rooij, D.G., van Pelt, A.M., and Page, D.C. (2008). Stra8 and its inducer, retinoic acid, regulate meiotic initiation in both spermatogenesis and oogenesis in mice. Proc. Natl. Acad. Sci. USA *105*, 14976–14980.

Baltus, A.E., Menke, D.B., Hu, Y.C., Goodheart, M.L., Carpenter, A.E., de Rooij, D.G., and Page, D.C. (2006). In germ cells of mouse embryonic ovaries, the decision to enter meiosis precedes premeiotic DNA replication. Nat. Genet. *38*, 1430–1434.

Berta, D.G., Kuisma, H., Välimäki, N., Räisänen, M., Jäntti, M., Pasanen, A., Karhu, A., Kaukomaa, J., Taira, A., Cajuso, T., et al. (2021). Deficient H2A.Z deposition is associated with genesis of uterine leiomyoma. Nature *596*, 398–403.

Bowles, J., Knight, D., Smith, C., Wilhelm, D., Richman, J., Mamiya, S., Yashiro, K., Chawengsaksophak, K., Wilson, M.J., Rossant, J., et al. (2006). Retinoid signaling determines germ cell fate in mice. Science *312*, 596–600.

Buaas, F.W., Kirsh, A.L., Sharma, M., McLean, D.J., Morris, J.L., Griswold, M.D., de Rooij, D.G., and Braun, R.E. (2004). Plzf is required in adult male germ cells for stem cell self-renewal. Nat. Genet. *36*, 647–652.

Cai, Y., Jin, J., Florens, L., Swanson, S.K., Kusch, T., Li, B., Workman, J.L., Washburn, M.P., Conaway, R.C., and Conaway, J.W. (2005). The mammalian YL1 protein is a shared subunit of the TRRAP/TIP60 histone acetyltransferase and SRCAP complexes. J. Biol. Chem. *280*, 13665–13670.

Chen, P., Zhao, J., Wang, Y., Wang, M., Long, H., Liang, D., Huang, L., Wen, Z., Li, W., Li, X., et al. (2013). H3.3 actively marks enhancers and primes gene transcription via opening higher-ordered chromatin. Genes Dev. *27*, 2109–2124.

Chen, Y., Zheng, Y., Gao, Y., Lin, Z., Yang, S., Wang, T., Wang, Q., Xie, N., Hua, R., Liu, M., et al. (2018). Single-cell RNA-seq uncovers dynamic processes and critical regulators in mouse spermatogenesis. Cell Res. *28*, 879–896.

Clapier, C.R., and Cairns, B.R. (2009). The biology of chromatin remodeling complexes. Annu. Rev. Biochem. *78*, 273–304.

Costoya, J.A., Hobbs, R.M., Barna, M., Cattoretti, G., Manova, K., Sukhwani, M., Orwig, K.E., Wolgemuth, D.J., and Pandolfi, P.P. (2004). Essential role of Plzf in maintenance of spermatogonial stem cells. Nat. Genet. *36*, 653–659.

Cuadrado, A., Corrado, N., Perdiguero, E., Lafarga, V., Muñoz-Canoves, P., and Nebreda, A.R. (2010). Essential role of p18Hamlet/SRCAP-mediated histone H2A.Z chromatin incorporation in muscle differentiation. EMBO J. *29*, 2014–2025.

Endo, T., Mikedis, M.M., Nicholls, P.K., Page, D.C., and de Rooij, D.G. (2019). Retinoic acid and germ cell development in the ovary and testis. Biomolecules *9*, 775.

Faast, R., Thonglairoam, V., Schulz, T.C., Beall, J., Wells, J.R.E., Taylor, H., Matthaei, K., Rathjen, P.D., Tremethick, D.J., and Lyons, I. (2001). Histone variant H2A.Z is required for early mammalian development. Curr. Biol. *11*, 1183–1187.

Feng, C.W., Bowles, J., and Koopman, P. (2014). Control of mammalian germ cell entry into meiosis. Mol. Cell. Endocrinol. *382*, 488–497.

Feng, Y., Tian, Y., Wu, Z., and Xu, Y. (2018). Cryo-EM structure of human SRCAP complex. Cell Res. *28*, 1121–1123.

Gallardo, T., Shirley, L., John, G.B., and Castrillon, D.H. (2007). Generation of a germ cell-specific mouse transgenic Cre line, *Vasa-Cre*. Genesis *45*, 413–417.

Giaimo, B.D., Ferrante, F., Herchenröther, A., Hake, S.B., and Borggrefe, T. (2019). The histone variant H2A.Z in gene regulation. Epigenetics Chromatin *12*, 37.

Greenberg, R.S., Long, H.K., Swigut, T., and Wysocka, J. (2019). Single amino acid change underlies distinct roles of H2A.Z subtypes in human syndrome. Cell *178*, 1421.e24–1436.e24.

Guo, J., Grow, E.J., Mlcochova, H., Maher, G.J., Lindskog, C., Nie, X., Guo, Y., Takei, Y., Yun, J., Cai, L., et al. (2018). The adult human testis transcriptional cell atlas. Cell Res. *28*, 1141–1157.

Guo, J., Grow, E.J., Yi, C., Mlcochova, H., Maher, G.J., Lindskog, C., Murphy, P.J., Wike, C.L., Carrell, D.T., Goriely, A., et al. (2017). Chromatin and single-cell RNA-seq profiling reveal dynamic signaling and metabolic transitions during human spermatogonial stem cell development. Cell Stem Cell *21*, 533.e6–546.e6.

Hammoud, S.S., Low, D.H., Yi, C., Carrell, D.T., Guccione, E., and Cairns, B.R. (2014). Chromatin and transcription transitions of mammalian adult germline stem cells and spermatogenesis. Cell Stem Cell *15*, 239–253.

Handel, M.A., and Schimenti, J.C. (2010). Genetics of mammalian meiosis: regulation, dynamics and impact on fertility. Nat. Rev. Genet. *11*, 124–136.

He, Y., Fang, J., Taatjes, D.J., and Nogales, E. (2013). Structural visualization of key steps in human transcription initiation. Nature *495*, 481–486.

Heinz, S., Benner, C., Spann, N., Bertolino, E., Lin, Y.C., Laslo, P., Cheng, J.X., Murre, C., Singh, H., and Glass, C.K. (2010). Simple combinations of lineage-determining transcription factors prime *cis*-regulatory elements required for macrophage and B cell identities. Mol. Cell *38*, 576–589.

Hermann, B.P., Cheng, K., Singh, A., Roa-De La Cruz, L., Mutoji, K.N., Chen, I.C., Gildersleeve, H., Lehle, J.D., Mayo, M., Westernströer, B., et al. (2018). The mammalian spermatogenesis single-cell transcriptome, from spermatogonial stem cells to spermatids. Cell Rep. *25*, 1650.e8–1667.e8.

Herrera-Cruz, M., Cruz, G., Valadez-Graham, V., Fregoso-Lomas, M., Villicaña, C., Vázquez, M., Reynaud, E., and Zurita, M. (2012). Physical and functional interactions between *Drosophila* homologue of Swc6/p18Hamlet subunit of the SWR1/SRCAP chromatin-remodeling complex with the DNA repair/transcription factor TFIIH. J. Biol. Chem. *287*, 33567–33580.

Hood, R.L., Lines, M.A., Nikkel, S.M., Schwartzentruber, J., Beaulieu, C., Nowaczyk, M.J., Allanson, J., Kim, C.A., Wieczorek, D., Moilanen, J.S., et al. (2012). Mutations in SRCAP, encoding SNF2-related crebbp activator protein, cause floating-harbor syndrome. Am. J. Hum. Genet. *90*, 308–313.

Ishiguro, K.I., Matsuura, K., Tani, N., Takeda, N., Usuki, S., Yamane, M., Sugimoto, M., Fujimura, S., Hosokawa, M., Chuma, S., et al. (2020). MEIOSIN directs the switch from mitosis to meiosis in mammalian germ cells. Dev. Cell *52*, 429.e10–445.e10.

Kaya-Okur, H.S., Wu, S.J., Codomo, C.A., Pledger, E.S., Bryson, T.D., Henikoff, J.G., Ahmad, K., and Henikoff, S. (2019). CUT&Tag for efficient epigenomic profiling of small samples and single cells. Nat. Commun. *10*, 1930.

Kimble, J. (2011). Molecular regulation of the mitosis/meiosis decision in multicellular organisms. Cold Spring Harb. Perspect. Biol. *3*, a002683.

Kimmins, S., and Sassone-Corsi, P. (2005). Chromatin remodelling and epigenetic features of germ cells. Nature *434*, 583–589.

Kobor, M.S., Venkatasubrahmanyam, S., Meneghini, M.D., Gin, J.W., Jennings, J.L., Link, A.J., Madhani, H.D., and Rine, J. (2004). A protein complex containing the conserved Swi2/Snf2-related ATPase Swr1p deposits histone variant H2A.Z into euchromatin. PLoS Biol. *2*, E131.

Kojima, M.L., de Rooij, D.G., and Page, D.C. (2019). Amplification of a broad transcriptional program by a common factor triggers the meiotic cell cycle in mice. eLife *8*, e43738.

Kota, S.K., and Feil, R. (2010). Epigenetic transitions in germ cell development and meiosis. Dev. Cell *19*, 675–686.

Koubova, J., Menke, D.B., Zhou, Q., Capel, B., Griswold, M.D., and Page, D.C. (2006). Retinoic acid regulates sex-specific timing of meiotic initiation in mice. Proc. Natl. Acad. Sci. USA *103*, 2474–2479.

Krogan, N.J., Baetz, K., Keogh, M.C., Datta, N., Sawa, C., Kwok, T.C., Thompson, N.J., Davey, M.G., Pootoolal, J., Hughes, T.R., et al. (2004). Regulation of chromosome stability by the histone H2A variant Htz1, the Swr1 chromatin remodeling complex, and the histone acetyltransferase NuA4. Proc. Natl. Acad. Sci. USA *101*, 13513–13518.

Langmead, B., Trapnell, C., Pop, M., and Salzberg, S.L. (2009). Ultrafast and memory-efficient alignment of short DNA sequences to the human genome. Genome Biol. *10*, R25.

Latendresse, J.R., Warbrittion, A.R., Jonassen, H., and Creasy, D.M. (2002). Fixation of testes and eyes using a modified Davidson's fluid: comparison with Bouin's fluid and conventional Davidson's fluid. Toxicol. Pathol. *30*, 524–533.

Lin, Y., Gill, M.E., Koubova, J., and Page, D.C. (2008). Germ cell-intrinsic and -extrinsic factors govern meiotic initiation in mouse embryos. Science *322*, 1685–1687.

Love, M.I., Huber, W., and Anders, S. (2014). Moderated estimation of fold change and dispersion for RNA-seq data with DESeq2. Genome Biol. *15*, 550.

Maezawa, S., Hasegawa, K., Yukawa, M., Sakashita, A., Alavattam, K.G., Andreassen, P.R., Vidal, M., Koseki, H., Barski, A., and Namekawa, S.H. (2017). Polycomb directs timely activation of germline genes in spermatogenesis. Genes Dev. *31*, 1693–1703.

Maezawa, S., Sakashita, A., Yukawa, M., Chen, X., Takahashi, K., Alavattam, K.G., Nakata, I., Weirauch, M.T., Barski, A., and Namekawa, S.H. (2020). Super-enhancer switching drives a burst in gene expression at the mitosis-to-meiosis transition. Nat. Struct. Mol. Biol. *27*, 978–988.

Maezawa, S., Yukawa, M., Alavattam, K.G., Barski, A., and Namekawa, S.H. (2018). Dynamic reorganization of open chromatin underlies diverse transcriptomes during spermatogenesis. Nucleic Acids Res. *46*, 593–608.

Matson, C.K., Murphy, M.W., Griswold, M.D., Yoshida, S., Bardwell, V.J., and Zarkower, D. (2010). The mammalian doublesex homolog DMRT1 is a transcriptional gatekeeper that controls the mitosis versus meiosis decision in male germ cells. Dev. Cell *19*, 612–624.

Mizuguchi, G., Shen, X., Landry, J., Wu, W.H., Sen, S., and Wu, C. (2004). ATP-driven exchange of histone H2AZ variant catalyzed by SWR1 chromatin remodeling complex. Science *303*, 343–348.

Mortazavi, A., Williams, B.A., McCue, K., Schaeffer, L., and Wold, B. (2008). Mapping and quantifying mammalian transcriptomes by RNA-seq. Nat. Methods *5*, 621–628.

Murphy, P.J., Wu, S.F., James, C.R., Wike, C.L., and Cairns, B.R. (2018). Placeholder nucleosomes underlie germline-to-embryo DNA methylation reprogramming. Cell *172*, 993.e13–1006.e13.

Nakagawa, T., Sharma, M., Nabeshima, Y., Braun, R.E., and Yoshida, S. (2010). Functional hierarchy and reversibility within the murine spermatogenic stem cell compartment. Science *328*, 62–67.

Raz, E. (2000). The function and regulation of vasa-like genes in germ-cell development. Genome Biol. *1*, REVIEWS1017.

Robinson, J.T., Thorvaldsdóttir, H., Winckler, W., Guttman, M., Lander, E.S., Getz, G., and Mesirov, J.P. (2011). Integrative genomics viewer. Nat. Biotechnol. *29*, 24–26.

Romer, K.A., de Rooij, D.G., Kojima, M.L., and Page, D.C. (2018). Isolating mitotic and meiotic germ cells from male mice by developmental synchronization, staging, and sorting. Dev. Biol. *443*, 19–34.

Ruhl, D.D., Jin, J., Cai, Y., Swanson, S., Florens, L., Washburn, M.P., Conaway, R.C., Conaway, J.W., and Chrivia, J.C. (2006). Purification of a human SRCAP complex that remodels chromatin by incorporating the histone variant H2A.Z into nucleosomes. Biochemistry *45*, 5671–5677.

Schneider, C.A., Rasband, W.S., and Eliceiri, K.W. (2012). NIH Image to ImageJ: 25 years of image analysis. Nat. Methods *9*, 671–675.

Schultz, N., Hamra, F.K., and Garbers, D.L. (2003). A multitude of genes expressed solely in meiotic or postmeiotic spermatogenic cells offers a myriad of contraceptive targets. Proc. Natl. Acad. Sci. USA *100*, 12201–12206.

Shi, Y., Fan, W., Xu, M., Lin, X., Zhao, W., and Yang, Z. (2022). Critical role of Znhit1 for post-natal heart function and vacuolar cardiomyopathy. JCI Insight, e148752. https://doi.org/10.1172/jci.insight.148752.

Sin, H.S., Kartashov, A.V., Hasegawa, K., Barski, A., and Namekawa, S.H. (2015). Poised chromatin and bivalent domains facilitate the mitosis-to-meiosis transition in the male germline. BMC Biol. *13*, 53.

Soh, Y.Q., Junker, J.P., Gill, M.E., Mueller, J.L., van Oudenaarden, A., and Page, D.C. (2015). A gene regulatory program for meiotic prophase in the fetal ovary. PLoS Genet. *11*, e1005531.

Stuart, T., Butler, A., Hoffman, P., Hafemeister, C., Papalexi, E., Mauck, W.M., 3rd, Hao, Y., Stoeckius, M., Smibert, P., and Satija, R. (2019). Comprehensive integration of single-cell data. Cell *177*, 1888.e21–1902.e21.

Subramanian, A., Tamayo, P., Mootha, V.K., Mukherjee, S., Ebert, B.L., Gillette, M.A., Paulovich, A., Pomeroy, S.L., Golub, T.R., Lander, E.S., and Mesirov, J.P. (2005). Gene set enrichment analysis: a knowledge-based approach for interpreting genome-wide expression profiles. Proc. Natl. Acad. Sci. USA *102*, 15545–15550.

Subramanian, V., Fields, P.A., and Boyer, L.A. (2015). H2A.Z: a molecular rheostat for transcriptional control. F1000Prime Rep. *7*, 01.

Sun, S., Jiang, N., Jiang, Y., He, Q., He, H., Wang, X., Yang, L., Li, R., Liu, F., Lin, X., and Zhao, B. (2020). Chromatin remodeler Znhit1 preserves

hematopoietic stem cell quiescence by determining the accessibility of distal enhancers. Leukemia *34*, 3348–3358.

Suzuki, A., Hirasaki, M., Hishida, T., Wu, J., Okamura, D., Ueda, A., Nishimoto, M., Nakachi, Y., Mizuno, Y., Okazaki, Y., et al. (2016). Loss of MAX results in meiotic entry in mouse embryonic and germline stem cells. Nat. Commun. *7*, 11056.

Suzuki, A., and Saga, Y. (2008). Nanos2 suppresses meiosis and promotes male germ cell differentiation. Genes Dev. *22*, 430–435.

Talbert, P.B., and Henikoff, S. (2017). Histone variants on the move: substrates for chromatin dynamics. Nat. Rev. Mol. Cell Biol. *18*, 115–126.

Tong, M.H., Yang, Q.E., Davis, J.C., and Griswold, M.D. (2013). Retinol dehydrogenase 10 is indispensible for spermatogenesis in juvenile males. Proc. Natl. Acad. Sci. USA *110*, 543–548.

Trapnell, C., Pachter, L., and Salzberg, S.L. (2009). TopHat: discovering splice junctions with RNA-seq. Bioinformatics *25*, 1105–1111.

Wang, M., Liu, X., Chang, G., Chen, Y., An, G., Yan, L., Gao, S., Xu, Y., Cui, Y., Dong, J., et al. (2018a). Single-cell RNA sequencing analysis reveals sequential cell fate transition during human spermatogenesis. Cell Stem Cell *23*, 599.e4–614.e4.

Wang, Y., Long, H., Yu, J., Dong, L., Wassef, M., Zhuo, B., Li, X., Zhao, J., Wang, M., Liu, C., et al. (2018b). Histone variants H2A.Z and H3.3 coordinately regulate PRC2-dependent H3K27me3 deposition and gene expression regulation in mES cells. BMC Biol. *16*, 107.

Wang, Y., Wang, H., Zhang, Y., Du, Z., Si, W., Fan, S., Qin, D., Wang, M., Duan, Y., Li, L., et al. (2019a). Reprogramming of meiotic chromatin architecture during spermatogenesis. Mol. Cell *73*, 547.e6–561.e6.

Wang, Z., Xu, X., Li, J.L., Palmer, C., Maric, D., and Dean, J. (2019b). Sertoli cell-only phenotype and scRNA-seq define PRAMEF12 as a factor essential for spermatogenesis in mice. Nat. Commun. *10*, 5196.

Wen, L., and Tang, F. (2019). Human germline cell development: from the perspective of single-cell sequencing. Mol. Cell *76*, 320–328.

Willhoft, O., Ghoneim, M., Lin, C.-L., Chua, E.Y.D., Wilkinson, M., Chaban, Y., Ayala, R., McCormack, E.A., Ocloo, L., Rueda, D.S., and Wigley, D.B. (2018). Structure and dynamics of the yeast SWR1-nucleosome complex. Science *362*, eaat7716.

Wong, M.M., Cox, L.K., and Chrivia, J.C. (2007). The chromatin remodeling protein, SRCAP, is critical for deposition of the histone variant H2A.Z at promoters. J. Biol. Chem. *282*, 26132–26139.

Wu, T., Lyu, R., You, Q., and He, C. (2020). Kethoxal-assisted single-stranded DNA sequencing captures global transcription dynamics and enhancer activity in situ. Nat. Methods *17*, 515–523.

Xu, M., Yao, J., Shi, Y., Yi, H., Zhao, W., Lin, X., and Yang, Z. (2021). The SRCAP chromatin remodeling complex promotes oxidative metabolism during prenatal heart development. Development *148*, dev199026.

Yadav, T., Quivy, J.P., and Almouzni, G. (2018). Chromatin plasticity: a versatile landscape that underlies cell fate and identity. Science *361*, 1332–1336.

Ye, B., Liu, B., Yang, L., Huang, G., Hao, L., Xia, P., Wang, S., Du, Y., Qin, X., Zhu, P., et al. (2017). Suppression of SRCAP chromatin remodelling complex and restriction of lymphoid lineage commitment by Pcid2. Nat. Commun. *8*, 1518.

Yokobayashi, S., Liang, C.Y., Kohler, H., Nestorov, P., Liu, Z., Vidal, M., van Lohuizen, M., Roloff, T.C., and Peters, A.H. (2013). PRC1 coordinates timing of sexual differentiation of female primordial germ cells. Nature *495*, 236–240.

Yue, F., Cheng, Y., Breschi, A., Vierstra, J., Wu, W., Ryba, T., Sandstrom, R., Ma, Z., Davis, C., Pope, B.D., et al. (2014). A comparative encyclopedia of DNA elements in the mouse genome. Nature *515*, 355–364.

Zhang, X., Gunewardena, S., and Wang, N. (2021). Nutrient restriction synergizes with retinoic acid to induce mammalian meiotic initiation in vitro. Nat. Commun. *12*, 1758.

Zhang, Y., Liu, T., Meyer, C.A., Eeckhoute, J., Johnson, D.S., Bernstein, B.E., Nusbaum, C., Myers, R.M., Brown, M., Li, W., et al. (2008). Model-based analysis of ChIP-seq (MACS). Genome Biol. *9*, R137.

Zhao, B., Chen, Y., Jiang, N., Yang, L., Sun, S., Zhang, Y., Wen, Z., Ray, L., Liu, H., Hou, G., and Lin, X. (2019). Znhit1 controls intestinal stem cell maintenance by regulating H2A.Z incorporation. Nat. Commun. *10*, 1071.

STAR★METHODS

KEY RESOURCES TABLE

Reagent or resource	Source	Identifier
Antibodies		
Rabbit polyclonal anti-Ddx4	Abcam	Cat#ab13840; RRID: AB_443012
Goat polyclonal anti-Dazl	Novus Biologicals	Cat#NB100-2437; RRID: AB_2089071
Goat polyclonal anti-Plzf	R&D Systems	Cat#AF2944; RRID: AB_2218943
Rabbit polyclonal anti-SOX9	Millipore	Cat#ABE571
Goat polyclonal anti-GFRα1	R&D Systems	Cat#AF714; RRID: AB_355541
Goat polyclonal anti-Kit	R&D Systems	Cat#AF1356; RRID: AB_354750
Rabbit polyclonal anti-Stra8	Abcam	Cat#ab49405; RRID: AB_945677
Mouse monoclonal anti-γH2AX	BioLegend	Cat#613401; RRID: AB_315794
Mouse monoclonal anti-Sycp3	Abcam	Cat#ab97672; RRID: AB_10678841
Mouse monoclonal anti-BrdU	Millipore	Cat#MAB3510; RRID: AB_94897
APC/Cyanine7 anti-mouse CD117 (c-Kit)	BioLegend	Cat#135135; RRID: AB_2632808
Rabbit monoclonal anti-β-Actin	Cell Signaling Technology	Cat#4970; RRID: AB_2223172
Rabbit polyclonal anti-Znhit1	Sigma-Aldrich	Cat#HPA019043; RRID: AB_1859481
Rabbit polyclonal anti-H2A.Z	Abcam	Cat#ab4174; RRID: AB_304345
Chemicals, peptides, and recombinant proteins		
Neutral balsam mounting medium	ZSGB-Bio	Cat#ZLI-9516
Fluoromount-G mounting medium	Southern Biotech	Cat#0100-01
Fixable Viability Dye eFluor™ 455UV	eBioscience	Cat#65-0868-14
RIPA lysis buffer	Beyotime	Cat#P0013
Protease inhibitor cocktail	Sigma-Aldrich	Cat#P8340
5-Bromo-2'-deoxyuridine (BrdU)	Sigma-Aldrich	Cat#B5002
Collagenase IV	Thermo Fisher Scientific	Cat#17104019
Trypsin	Thermo Fisher Scientific	Cat#25200072
Lectin PNA (FITC Conjugate)	Sigma-Aldrich	Cat#L7381
N_3-kethoxal	C. He (University of Chicago)	N/A
Tn5 transposase	Abclonal	Cat#RK20547
ChIP-Grade Protein G Magnetic Beads	Cell Signaling Technology	Cat#9006
TruePrep Index Kit V2 for Illumina	Vazyme	Cat#TD202
Critical commercial assays		
RNAscope 2.5 kit	Advanced Cell Diagnostics	Cat#322310
RNeasy Plus Mini Kit	QIAGEN	Cat#74134
GoScript Reverse Transcription Kit	Promega	Cat#A5003
2 × SYBR Green qPCR Master Mix	Bimake	Cat#B21202
Pierce™ BCA kit	Thermo Fisher Scientific	Cat#23225
DNA Clean and Concentrator kit	Zymo	Cat#D4013
DNBeLAB V2 kit	BGI genomics	Cat#940-000047-00
DeadEnd™ Fluorometric TUNEL System	Promega	Cat#G3250
Hieff NGS® G-Type In-Situ DNA Binding Profiling Library Prep Kit	Yeasen Biotech	Cat#12598ES04
Deposited data		
RNA-seq data	This paper	SRP265368
ChIP-seq data	This paper	SRP265431
KAS-seq data	This paper	SRP361635
STRA8-FLAG ChIP-Seq data	(Kojima et al., 2019)	GEO GSE115928

(*Continued on next page*)

Continued

Reagent or resource	Source	Identifier
Experimental models: Organisms/strains		
Mouse: *Znhit1*$^{fl/fl}$	(Zhao et al., 2019)	N/A
Mouse: *Ddx4-cre*	The Jackson Laboratory	JAX: 006954
Oligonucleotides		
see Tables S4 and S5 for primers used in this study	This paper	N/A
Software and algorithms		
ImageJ (Version 1.52a)	(Schneider et al., 2012)	https://imagej.nih.gov/ij/
GraphPad Prism8	GraphPad Software	N/A
FV31S-SW Version: 2.1.1.98	Olympus	N/A
Fastqc	Babraham Bioinformatics	http://www.bioinformatics.babraham.ac.uk/projects/fastqc/
trim_galore	Babraham Bioinformatics	http://www.bioinformatics.babraham.ac.uk/projects/trim_galore/
TopHat v2.0.8	(Trapnell et al., 2009)	http://ccb.jhu.edu/software/tophat/index.shtml
Deseq	(Love et al., 2014)	https://github.com/mikelove/DESeq2
GSEA	(Subramanian et al., 2005)	http://www.gsea-msigdb.org/
Bowtie v1.1.1	(Langmead et al., 2009)	http://bowtie-bio.sourceforge.net/index.shtml
MACS	(Zhang et al., 2008)	http://github.com/taoliu/MACS
Seurat3	(Stuart et al., 2019)	https://satijalab.org/seurat/
Homer	(Heinz et al., 2010)	http://homer.ucsd.edu/homer/
Integrative Genomics Viewer	(Robinson et al., 2011)	http://www.broadinstitute.org/igv/; RRID: SCR_011793

RESOURCE AVAILABILITY

Lead contact

Further information and requests for resources and reagents should be directed to and will be fulfilled by the lead contact, Xinhua Lin (xlin@fudan.edu.cn).

Materials availability

Unique materials generated in this study are available from the lead contact without restriction.

Data and code availability

RNA-seq data, ChIP-seq data, and KAS-seq data have been deposited at the NCBI SRA database and are publicly available as of the date of publication. Accession numbers are listed in the key resources table. This paper does not report the original code. Any additional information required to reanalyze the data reported in this paper is available from the lead contact upon request.

EXPERIMENTAL MODEL AND SUBJECT DETAILS

Znhit1$^{fl/fl}$ mice were generated by the Model Animal Research Center of Nanjing University (MARC, Nanjing, China) (Zhao et al., 2019). *Ddx4-cre* mice were obtained from the Jackson Laboratory (Gallardo et al., 2007). All of the lines were maintained in the C57BL/6J background. Animal experiments were performed following relevant guidelines and approved by the Animal Care and Use Committee of Fudan University. All mice were housed in the SPF (Specific-Pathogen-Free) animal facility with standard 12 hours light/dark cycles and standard temperature (22 to 24°C). All mice were provided with ad libitum access to standard laboratory food and water.

For 5-Bromo-2'-deoxyuridine (BrdU) incorporation experiments, mice were intraperitoneally injected at 10 μL/g body weight with 10 mg/mL BrdU (Sigma-Aldrich) in PBS, 4 hours before they were sacrificed for analysis.

METHOD DETAILS

Histology

For histological analysis and immunofluorescence, testes were fixed using modified Davidson's fixative as previously described (Latendresse et al., 2002); 5 μm testes sections were prepared for periodic acid-Schiff (PAS)-hematoxylin staining or immunofluorescent staining. For PAS- hematoxylin staining, sections were deparaffinized, and incubated with 0.5% periodic acid solution for 5 min, then stained

with Schiff's reagent for 15 min, followed by counterstaining with hematoxylin solution for 5 min. Sections were mounted with neutral balsam mounting medium (ZSGB-Bio). For immunofluorescence, sections were treated for sodium citrate antigen retrieval, then blocked with 5% BSA in PBS for 30 min, and incubated overnight at 4°C with α-Ddx4 (ab13840, Abcam), α-Dazl (NB100-2437, Novus Biologicals), α-Plzf (AF2944, R&D), α-SOX9 (ABE571, Millipore), α-GFRα1 (AF714, R&D), α-Kit (AF1356, R&D), α-Stra8 (ab49405, Abcam), α-γH2AX (613401, BioLegend), α-Sycp3 (ab97672, Abcam), α-BrdU (MAB3510, Millipore), or Lectin PNA (FITC Conjugate, L7381, Sigma-Aldrich). A secondary fluorescein-conjugated antibody was added for 1 hour, followed by Fluoromount-G (Southern Biotech) mounting. Images were taken using an inverted microscope (IX73, Olympus) or confocal laser scanning microscope (FV3000, Olympus).

TUNEL assay

TUNEL assay was performed using the DeadEnd™ Fluorometric TUNEL System (Promega), according to the manufacturer's instructions. The number of TUNEL positive cells was counted for quantitative analysis.

RNAscope in situ hybridization

For *Znhit1* in situ hybridization, 5 μm testes sections were processed for in situ hybridization with the RNAscope 2.5 kit (Advanced Cell Diagnostics), according to the manufacturer's instructions.

Isolation of Kit$^+$ spermatogonia

Freshly harvested testes were digested using collagenase IV and trypsin. Dead cells were excluded by FVD eFluor® 455UV (eBioscience) staining. Single-cell suspensions prepared from testes were incubated for 30 min at 4°C with APC/Cyanine7 anti-mouse CD117 (c-kit) antibody (BioLegend). Flow cytometry was performed using FACSAria Fusion (BD) flow cytometer.

Quantitative RT-PCR (RT-qPCR)

RNA was extracted with RNeasy Plus Mini Kit (QIAGEN) and cDNA was reverse transcribed using the GoScript Reverse Transcription System (Promega). Quantitative PCR was performed using 2×SYBR Green qPCR Master Mix (Bimake) and amplification was quantified using the CFX-96 system (Bio-Rad). The primer sequences used are listed in Table S4.

Western blot

Freshly harvested testes were digested by RIPA lysis buffer (Beyotime) containing protease inhibitor cocktail (Sigma-Aldrich). Protein concentration was determined by the BCA kit (Thermo Fisher). Western blot was performed using the following antibodies: α-β-Actin (CST-4970, 1:1000), α-Znhit1 (Sigma-HPA019043, 1:100), α-H2A.Z antibody (Abcam-ab4174, 1:100), and ECL HRP-conjugatedα-rabbit IgG. The band intensity was quantitated with ImageJ (Version 1.52a) (Schneider et al., 2012).

RNA-seq

RNA from fresh testes was converted into cDNA and then subjected to high-throughput sequencing. Over 40 million reads were obtained per sample using the Illumina Novaseq platform for 3 biological replicates. The RNA-seq data were mapped to the mm10 genome by TopHat v2.0.8 (Trapnell et al., 2009) with no more than 2 mismatches, and only uniquely mapped reads were used to estimate the expression values in gene level in terms of RPKM (Mortazavi et al., 2008). Statistical significance tests for differentially expressed genes were performed using DEseq in R (Love et al., 2014). Genes with absolute $\log_2$-transformed fold changes greater than 1.5 were regarded as differentially expressed genes and a threshold of p-value < 0.05 was used. GSEA was performed as published previously (Subramanian et al., 2005).

ChIP-seq and KAS-seq

For ChIP-seq, freshly harvested testes were digested by collagenase IV at 37°C for 10 min, then cross-linked with 1% formaldehyde for 10 min at room temperature, quenched with glycine, and successively washed with cold PBS. The cells were lysed and sheared with a Bioruptor Plus for 20 min. For each ChIP, 100 μL of the sonicated chromatin was diluted using 0.06% SDS, incubated with 2 μg of α-H2A.Z antibody (ab4174, Abcam), and then 20 μL of protein G magnetic beads were added (Cell Signaling Technology) overnight at 4°C. The beads were washed with RIPA buffer and then LiCl buffer. After successive washes, chromatin was incubated at 65°C for 4 h to reverse crosslink, followed by incubation with proteinase K at 55°C for 2 h. DNA was purified and subjected to ChIP-seq. For KAS-seq, freshly harvested testes were digested using collagenase IV and trypsin, followed by labeling with N3-kethoxal. Genomic DNA was isolated using the DNA Clean and Concentrator kit (Zymo) and was fragmented using Tn5 transposase (ABclonal) as previously described (Wu et al., 2020). For high-throughput sequencing, over 30 million reads were obtained per sample on the Illumina Novaseq platform by BerryGenomics. Sequencing reads were aligned to a reference genome (mm10) using Bowtie v1.1.1 (Langmead et al., 2009) with no more than 2 mismatches, and then only the uniquely mapped reads were used for peak calling analysis. Peak detection was performed using MACS with default cutoffs (Zhang et al., 2008). Peaks were assigned to the nearest genes using Homer (Heinz et al., 2010). Tracks were visualized using Integrative Genomics Viewer (Robinson et al., 2011). ChIP-seq data for Stra8 in testes were reported previously by Kojima et al. (Kojima et al., 2019).

CUT&Tag

Kit$^+$ cells were sorted and were then subjected to perform CUT&Tag assay as previously described (Kaya-Okur et al., 2019). In brief, 40,000 Kit$^+$ cells were harvested and washed twice in washing buffer (20 mM HEPES pH 7.5; 150 mM NaCl; 0.5 mM Spermidine; 1×Protease inhibitor cocktail), then incubated with activated Concanavalin A coated magnetic beads. 0.5 μg α-H2A.Z antibody (ab4174, Abcam) was added and incubated on a rotating platform at room temperature for 2 h. Then, 0.5 μL Goat anti-Rabbit secondary antibody was added and incubated for 30 min. After washing, cells were segmented with pA/G-Tn5 transposase (12598ES04, Yeasen Biotech) at 37°C for 1 h. After 30 min incubation with proteinase K at 55 °C, DNA was extracted and was then subjected to quantitative PCR. For quantitative analysis, 5 pg E. coli Lambda DNA was added as DNA spike-in. The primer sequences used are listed in Table S5.

Single-cell RNA sequencing (scRNA-seq)

Freshly harvested testes were digested using collagenase IV and trypsin. Live testicular cells were sorted and were then subjected to perform scRNA-seq with the DNBeLAB V2 kit (BGI genomics), according to the manufacturer's instructions. The raw sequencing data were analyzed by the DNBeLAB C2 scRNA v2.3 (BGI genomics) to generate the gene expression containing UMIs (unique molecular identifies) matrix with default parameters. The gene expression UMIs matrix was further analyzed by Seurat3 (Stuart et al., 2019). Cells with more than 200 genes and the genes, which were expressed in at least 3 cells, were used to create Seurat objects. The first 50 principal components were used for the t-SNE (t-distributed Stochastic Neighbor Embedding) and UMAP (Uniform Manifold Approximation and Projection) analysis to find the cell clusters. Cluster identity was assigned by manual annotation using known marker genes.

QUANTIFICATION AND STATISTICAL ANALYSIS

Data are shown as the mean ± s.d. For comparative analysis, an unpaired Student's two-tailed *t*-test was used and results were graphed using GraphPad Prism8.